

In-situ oxide coatings improve atom probe tomography analysis of silica-embedded model protein DegP

Downloaded from: https://research.chalmers.se, 2026-11-28 03:56 UTC

Citation for the original published paper (version of record):

Mayweg, D., Eriksson, G., Stepulane, A. et al (2026). In-situ oxide coatings improve atom probe tomography analysis of silica-embedded model protein
DegP. Advances in Sample Preparation, 20. http://dx.doi.org/10.1016/j.sampre.2026.100262

N.B. When citing this work, cite the original published paper.

research.chalmers.se offers the possibility of retrieving research publications produced at Chalmers University of Technology. It covers all kind of research output: articles, dissertations, conference papers, reports etc. since 2004. research.chalmers.se is administrated and maintained by Chalmers Library

(article starts on next page)

Advances in Sample Preparation 20 (2026) 100262

Contents lists available at ScienceDirect

Advances in Sample Preparation

journal homepage: www.elsevier.com/locate/sampre

In-situ oxide coatings improve atom probe tomography analysis of silica-embedded model protein DegP

David Mayweg [a,b,**], Gustav Eriksson [a,c,d], Annija Stepulane [a], Darius Šulskis [e,f], Björn M. Burmann [e,g], Per Malmberg [h], Mattias Thuvander [b], Mats Hulander [c], Martin Andersson [c,*]

[a] Vitroprobe Analytics AB, Gothenburg, Sweden
[b] Department of Physics and Astronomy, Division of Microstructure Physics, Chalmers University of Technology, Gothenburg, Sweden
[c] Department of Chemistry and Chemical Engineering, Division of Applied Chemistry, Chalmers University of Technology, Gothenburg, Sweden
[d] Max Planck Institute for Sustainable Materials, Department of Circular Metallurgy and Alloy Design, 40237 Düsseldorf, Germany
[e] Department of Chemistry and Molecular Biology and the Wallenberg Centre for Molecular and Translational Medicine, University of Gothenburg, Sweden
[f] Institute of Biotechnology, Life Sciences Center, Vilnius University, Vilnius, Lithuania
[g] Swedish NMR Centre, Science for Life Laboratory Integrated Structural Biology Platform, University of Gothenburg, Sweden
[h] Department of Chemistry and Chemical Engineering, Division of Chemistry and Biochemistry, Chalmers University of Technology, Gothenburg, Sweden

ARTICLE INFO

Keywords:
Atom probe tomography
Nano-scale characterization
Protein
sol-gel silica

ABSTRACT

Here, we demonstrate how *in situ* alumina and chromia coatings improve data quality in atom probe analyses of ^{13}C-labelled protein DegP embedded in porous silica *via* a sol–gel process. The coatings promote more homogeneous evaporation, resulting in smoother voltage curves, which is one prerequisite for reliable reconstructions. Furthermore, a key challenge associated with embedding proteins in silica is the pick-up of contaminant carbon originating from sources other than the protein of interest. By applying oxide coatings, this contamination is substantially reduced, resulting in a measured ^{13}C fraction above 90 % in most cases and above 95 % in many cases. The use of such coatings therefore improves the ability to distinguish protein-derived signals from background contamination and could improve the analysis of non-isotopically labelled proteins. These results demonstrate that *in situ* oxide coatings represent a promising approach for improving sample quality and analytical performance in atom probe studies of proteins embedded in porous silica.

1. Introduction

Structural and chemical characterization of proteins is essential both for advancing our fundamental understanding of biological systems and for the effective development of new pharmaceuticals. Direct three dimensional (3D) structural imaging of individual proteins and interactions between individual proteins are therefore of great importance.

Although protein structure determination is routinely performed using X-ray diffraction (XRD), the technique is strictly limited to analysis of crystallized proteins. For conventional measurements, crystals several tens of micrometres in size are typically preferred [1]. However, many proteins of pharmaceutical relevance do not readily form suitable crystals. In such cases, transmission electron microscopy (TEM) imaging at cryogenic conditions (cryo-EM), combined with single-particle analysis, can be employed. Cryo-EM remains challenging for small proteins, particularly those below approximately 50 kDa [2]. For such analysis proteins must be captured in vitrified buffer solutions, where they should be homogenously distributed and must be randomly oriented, and the resulting sample must be sufficiently thin to be electron transparent. Useful data can be obtained from as little as 1000 protein micrographs via single particle analysis. To obtain the highest resolution a large number of protein particles (several tens of thousands to more than a million [3]) need to be obtained under identical conditions, which rules out studies of, e.g., intrinsically disordered proteins. Another established technique in structural biology is nuclear magnetic resonance (NMR) spectroscopy, which is primarily applied to characterize proteins smaller than approximately 30 kDa [4]. Unlike XRD and

* Corresponding author.
** Corresponding author at: Department of Physics and Astronomy, Division of Microstructure Physics, Chalmers University of Technology, Gothenburg, Sweden.
E-mail addresses: david.mayweg@gmail.com (D. Mayweg), Martin.Andersson@chalmers.se (M. Andersson).

https://doi.org/10.1016/j.sampre.2026.100262
Received 12 September 2026; Received in revised form 27 October 2026; Accepted 14 November 2026
Available online 22 November 2026
2772-5820/© 2026 The Authors. Published by Elsevier B.V. This is an open access article under the CC BY license (http://creativecommons.org/licenses/by/4.0/).

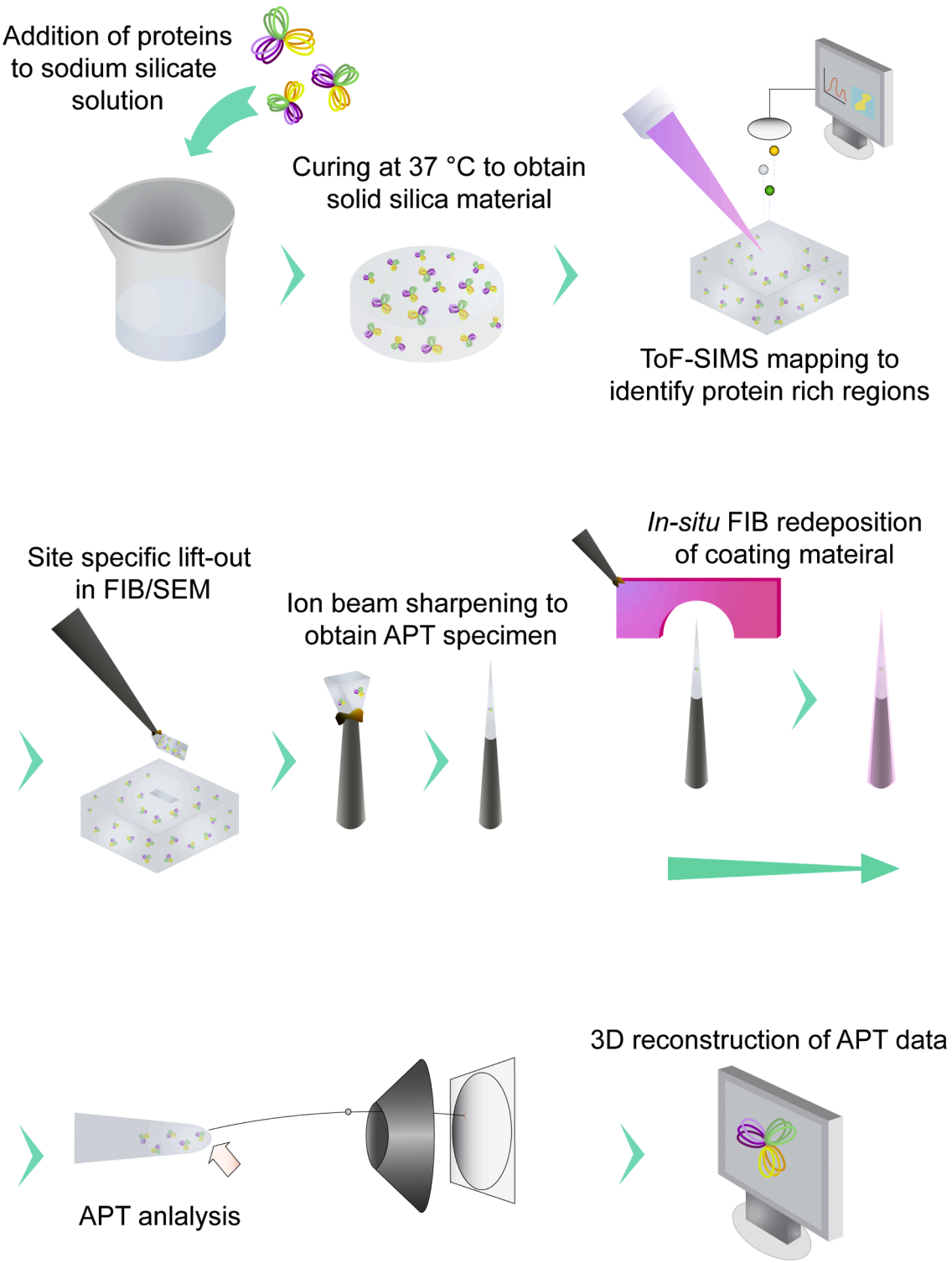

Fig. 1. Workflows conducted in this work. DegP-embedding in silica followed by ToF-SIMS mapping. FIB lift-out, specimen shaping and oxide coating as well as APT analysis and 3D reconstruction of oxide-coated and non-coated specimens.

cryo-EM, NMR can provide unique insight into intrinsically disordered proteins and dynamic states [5,6]. Its main limitation is that only nuclei with a non-zero nuclear spin are NMR active. Consequently, detailed structural information is obtained using isotopically labelled proteins like ^{13}C and ^{15}N [7].

In recent years, these experimental techniques have been complemented by machine learning models, such as AlphaFold, which have demonstrated unprecedented capability to predict high-resolution structural models across entire proteomes. Such models have become indispensable resources for generating new hypotheses in protein research. However, the obtained structural models remain more limited in predicting interactions between proteins, and experimental data is still required both to validate the predictions and to provide relevant training data.

Atom probe tomography (APT) is a nanoscale analytical technique mainly used in materials science and adjacent disciplines [8], although

its potential for the analysis of biological matter was envisaged by some of the pioneers of the technique several decades ago [9]. APT combines triggered field evaporation with time-of-flight measurements, which are converted into mass-to-charge ratios, thereby enabling 3D reconstructions of consecutively evaporated atoms while providing chemical identification of nearly every detected ion.

During an APT experiment, a needle-shaped specimen with a tip radius of a few tens of nanometres is maintained at cryogenic temperature (typically 30–70 K) in ultra-high vacuum (UHV), typically below 10^{-10} torr, and exposed to a standing electric field on the order of several tens of V/nm. The evaporation of individual atoms is triggered either by voltage pulses, which can be used for electrically conductive materials, or by femtosecond laser pulses. While the nature of the laser-matter interaction depends on both photon energy and material properties, it is generally accepted that, in most commercial APT instruments, evaporation is triggered by a thermal pulse induced by laser heating [10]. However, there are indications that, with increasing photon energy, other mechanisms might play a prominent role in laser-assisted field evaporation of materials with large bandgaps [11,12].

APT has the potential to complement established techniques routinely used in structural biology and organic chemistry by providing 3D real-space information with nm resolution and high chemical sensitivity. In particular, APT may enable analysis of proteins smaller than 50 kDa, which remain challenging for Cryo-EM [13], and even provide structural information from individual proteins to reveal structural heterogeneity [14]. Nevertheless, many challenges remain and need to be addressed before the technique can be effectively applied to protein characterization [15–17]. Similar to electron microscopy, the UHV environment in the atom probe instrument, as well as in the focused ion beam (FIB) used for specimen preparation, and the high electrostatic fields are unfavourable for maintaining protein integrity compared with physiological aqueous conditions at 37 °C.

Cryogenic workflows analogous to those used in cryo-EM represent one possible approach [15–18]. However, implementing such workflows for APT requires additional preparation steps and dedicated instrumentation during specimen preparation and transfer [19]. To circumvent some of these challenges, we employ a method in which proteins, here the bacterial serine protease DegP [20,21], were embedded in amorphous silica (SiO_2) using an aqueous sol-gel process [14,22,23]. All steps in the APT sample preparation workflow are performed between room temperature and 37 °C, thereby avoiding the need for vitrification and cryogenic specimen preparation strategies.

For reliable analyses, a homogenous distribution of proteins is required to enable the identification of individual proteins. On the other hand, relatively short inter-protein distances are necessary to ensure that enough proteins are present in any given APT specimen. APT does not require a particular distribution of protein orientations. Ideally, evaporation occurs atom by atom, or more precisely, ion by ion. However, at comparatively high laser pulse energies (LPEs), an increasing number of molecular ions are detected.

A significant challenge in APT studies of porous and heterogeneous materials is inhomogeneous evaporation across the specimen surface, which can lead to spikes in the detection rate and, consequently, a discontinuous voltage profile. Reliable reconstruction of a 3D volume using different algorithms, including voltage-based reconstruction [24], requires homogenous evaporation and a smooth increase in the applied voltage.

The workflow employed in the present work is illustrated schematically in Fig. 1. Following the embedding of the bacterial protease DegP, here the trimeric DegP variant $DegP^{Y444A}$, in silica (see Section 2.2), time-of-flight secondary ion mass spectrometry (ToF-SIMS) mapping was performed to identify regions containing significant amounts of protein. Specimen lift-out and sharpening were subsequently conducted using FIB milling, followed by *in-situ* oxide coating of selected specimens. The specimens were then transferred to the APT instrument for data acquisition (Section 2.5) and subsequent analysis.

2. Materials and methods

2.1. DegP preparation

For the present study, we used the constitutively trimeric DegP variant $DegP^{Y444A}$, hereafter referred to as DegP. The protein was expressed with an N-terminal His_6-Tag. For isotope labelling, the protein was expressed in minimal medium containing ^{13}C-glucose and $^{15}NH_4Cl$ as the sole carbon and nitrogen sources, respectively, as described earlier [20]. Following expression, DegP was purified according to an established protocol [20], which in short comprised Ni-NTA affinity chromatography under native conditions, followed by Ni-NTA affinity chromatography under denaturing conditions with on-column refolding, and a final size-exclusion chromatography step. Purified protein was pooled and flash frozen in liquid nitrogen.

2.2. DegP encapsulation in silica glass

An aqueous sodium silicate solution (26.9 wt% SiO_2, 8.2 wt% Na_2O, Supelco) was neutralized using a strong acid cation-exchange resin (AmberChrom™ 50WX8, 200–400 mesh, Supelco). Approximately 5 g of resin was packed into a glass chromatography column fitted with a fritted glass disc (23 ml, porosity grade 0) to prevent any resin throughflow and activated by washing with two column volumes of 4 M NaOH, followed by Milli-Q water until the eluate was clear. The resin was then converted to the H^+ form by washing with two column volumes of 1 M HCl, equilibrated for 15 min, and rinsed with water to remove any residual HCl until the eluate reached pH ~ 4.5.

The aqueous sodium silicate solution was further diluted with Milli-Q water at a 1:3 vol ratio (pH ~ 12) and introduced to the column in 1 ml increments. The first 4 ml of eluate were discarded to ensure steady-state neutralization, after which fractions were collected and continuously monitored for pH. Fractions with a pH of ~ 3 were pooled, whereas later fractions showed a rapid resin depletion with eluate returning to pH ~ 12. The neutralized waterglass sol (pH ~ 3) was filtered twice through a 0.2 μm PVDF syringe filter to remove any resin residues and stored on ice to prevent gelation. The sol was either used directly for protein embedding or adjusted to pH 4 – 5 with 0.5 M NaOH, with pH monitored using a pH meter, depending on the desired experimental conditions.

Uniformly ^{13}C-labelled *Escherichia coli* $DegP^{Y444A}$ mutant (46,737 Da per monomer) was used as a model protein for all embedding experiments. The protein solution (300 μM) was prepared in 25 mM potassium phosphate buffer containing 1 mM EDTA and 1 mM TCEP at pH 7.0. For silica encapsulation, the protein solution was added to the neutralized waterglass (pH ~4.5) at varying volume ratios (2 – 1 parts waterglass to 1 part protein) and mixed gently by pipetting in a glass vial. The resulting mixture (sol state) was either deposited as ~20 μl droplets onto clean microscope coverslips to form thin films or left in the vial to form bulk samples. Upon curing at 37 °C, the sol gradually transitioned into a gel, followed by drying and densification into an amorphous silica glass. Thin-film samples were cured for ~ 24 h, and bulk samples for 48 – 72 h, yielding protein-embedded amorphous silica matrices. The resulting protein-containing silica glass was mounted onto aluminium blocks and embedded in an epoxy matrix (EpoFix resin, Agar Scientific). Flat cross-sectional surfaces were prepared by manual grinding (SiC paper 120, 500, 1200 grit), followed by polishing with diamond suspensions (9, 3, and 1 μm).

2.3. ToF-SIMS mapping

ToF-SIMS measurements were performed using an *ION.TOF.SIMS*^{5} instrument equipped with a Bi liquid metal ion gun as the primary ion source. In spectrometry mode, primary ion currents of 0.4–0.5 pA were used, with a beam spot size of approximately 1 μm. Since the samples were non-conductive and were embedded in a non-conductive epoxy resin, charge compensation was applied using a combination of electron

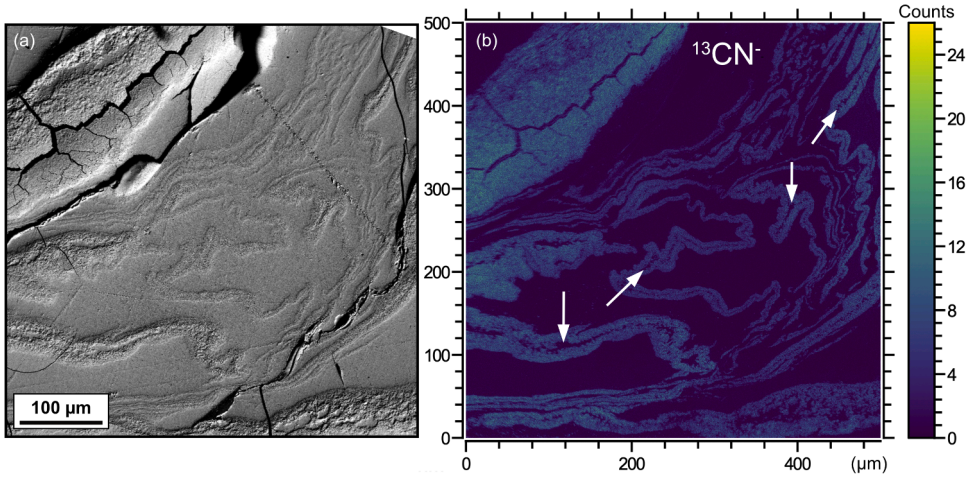

Fig. 2. (a) SEM image and (b) corresponding ToF-SIMS map of the $^{13}CN^-$ distribution in a silica sample containing ^{13}C-labelled DegP. The ToF-SIMS image was acquired in fast imaging mode to improve spatial resolution. The SEM image and ToF-SIMS map correspond to the same sample region. White arrows highlight regions attributed to phase separation.

flooding and stage biasing. The highest secondary ion count rates were obtained at stage biases of approximately 120–160 V, depending on the measurement location on the sample with respect to the sample edge. A substantial decrease in secondary-ion yield was observed when samples were kept in the vacuum inside the instrument for extended periods of time (e.g., overnight). Measurements were initially performed in *spectrometry mode*, which provides higher mass resolution ($m/\Delta m \approx 8000$) but lower spatial resolution than *fast-imaging mode* ($m/\Delta m$ ca. 100), to identify the most informative ionic species. Among the detected species, the molecular ions $^{13}CN^-$ and $^{13}CNO^-$ were found to be best suited for imaging, highlighting the regions with high DegP concentrations. Fast-imaging mode, with primary ion currents of 0.10–0.15 pA, was subsequently used to generate chemical maps with improved spatial resolution of approximately 75 nm.

2.4. Focused ion beam (FIB) specimen preparation

To minimize surface charging, the polished surfaces were sputter-coated with a ~10–20 nm Au layer. APT specimens were prepared using an FEI Versa3D dual beam SEM-FIB instrument for lift-out, mounting and final tip sharpening [25]. Since the silica specimens are beam-sensitive and prone to bending during electron beam imaging, the sharpening process was monitored using low currents and voltages (< 50 pA, 1–2 kV), low magnification and short dwell times (50 ns). Selected specimens were coated with metallic Cr, alumina or chromia using a procedure adopted from Schwarz et al. [26]. For the oxide coatings, deposition was performed using different angular sequences (0°/90° or 0°/90°/45°/135°) with a beam current of 30 pA at 30 kV and deposition times of 45–75 s per step. Owing to their comparatively lower sputter yield, the resulting oxide coatings were substantially thinner than the metallic Cr coatings. Due to the strong impact (bending) that EM-imaging has on the specimen in the final condition it was not possible to obtain useful images. Hence, the success of the coating process could only be determined by the APT measurements.

2.5. Atom probe tomography

APT experiments were performed using a Cameca LEAP 6000 XR (laser wavelength of 257.5 nm, detection efficiency 52 %) operated with a base temperature of 50 K and with LPEs ranging from 5 to 100 pJ (mostly 10–50 pJ) and a pulse repetition rate typically set to 100 kHz. In a limited number of measurements, higher repetition rates were used when elevated signals from CO^+ or H_x^+ species were detected, as shorter time intervals between pulses reduce the time available for adsorption of residual gas species. The target detection rate was set between 0.5 and 5 %. All datasets were reconstructed using the proprietary software package AP Suite 6.3 from Cameca. Each mass-to-charge spectrum was ranged individually, and peaks at 6, 12, 16, 32, and 69 Da, corresponding to $^{12}C^{++}$, $^{12}C^+$, $^{16}O^+$, $^{16}O_2^+$ and $^{69}Ga^+$, respectively, were used for mass calibration. Adsorption of residual hydrogen complicates the distinction between specimen-derived and background hydrogen in these specimens [27]. Consequently, no attempt was made to analyse the distributions of H^+, H_2^+, and H_3^+, which were commonly detected in the mass-to-charge spectra. Moreover, the spatial distribution of H was not required for the structural characterization of the proteins investigated here. Interpretation of the oxygen distribution was similarly challenging because oxygen-containing signals have multiple possible sources, including the silica matrix, embedded proteins and contamination, and were therefore not used as protein-specific markers. Therefore, these signals provide no chemical specificity for distinguishing the protein from the surrounding silica. Accordingly, the analysis focused primarily on selected atomic carbon ions associated with ^{13}C labelling.

3. Results and discussion

3.1. ToF-SIMS on samples with ^{13}C-labelled proteins

In many of the prepared silica samples, the proteins formed aggregates, resulting in spatially heterogeneous samples with protein-rich regions interspersed with regions consisting of virtually pure silica. While this aggregation complicates the identification of individual proteins in the APT datasets (see Section 3.4), it facilitates the localization of protein-rich regions at the sample surface using ToF-SIMS. The $^{13}CN^-$ signal was particularly useful for identifying regions with elevated protein concentration, whereas the $^{13}CN^-/^{12}CN^-$ ratio provided improved contrast at lower protein concentrations. Fig. 2a shows a secondary electron (SE) image of a silica sample containing DegP, while Fig. 2b presents the corresponding $^{13}CN^-$ ion map (see Figure S1 for a larger overview and Figure S 2 for maps of additional species, including $^{12}CN^-$). The sample was synthesised at a pH of 4 – 5, where relatively rapid gelation limited efficient mixing, thus hindering the formation of a homogenous protein distribution. In addition, partial phase separation was observed immediately after the addition of DegP solution to the pH-adjusted sodium silicate solution, further contributing to the inhomogeneous protein distribution. Additional phase separation appears to have occurred within the protein-rich regions during gelation, as indicated by distinct features in the central parts of the protein-rich layers

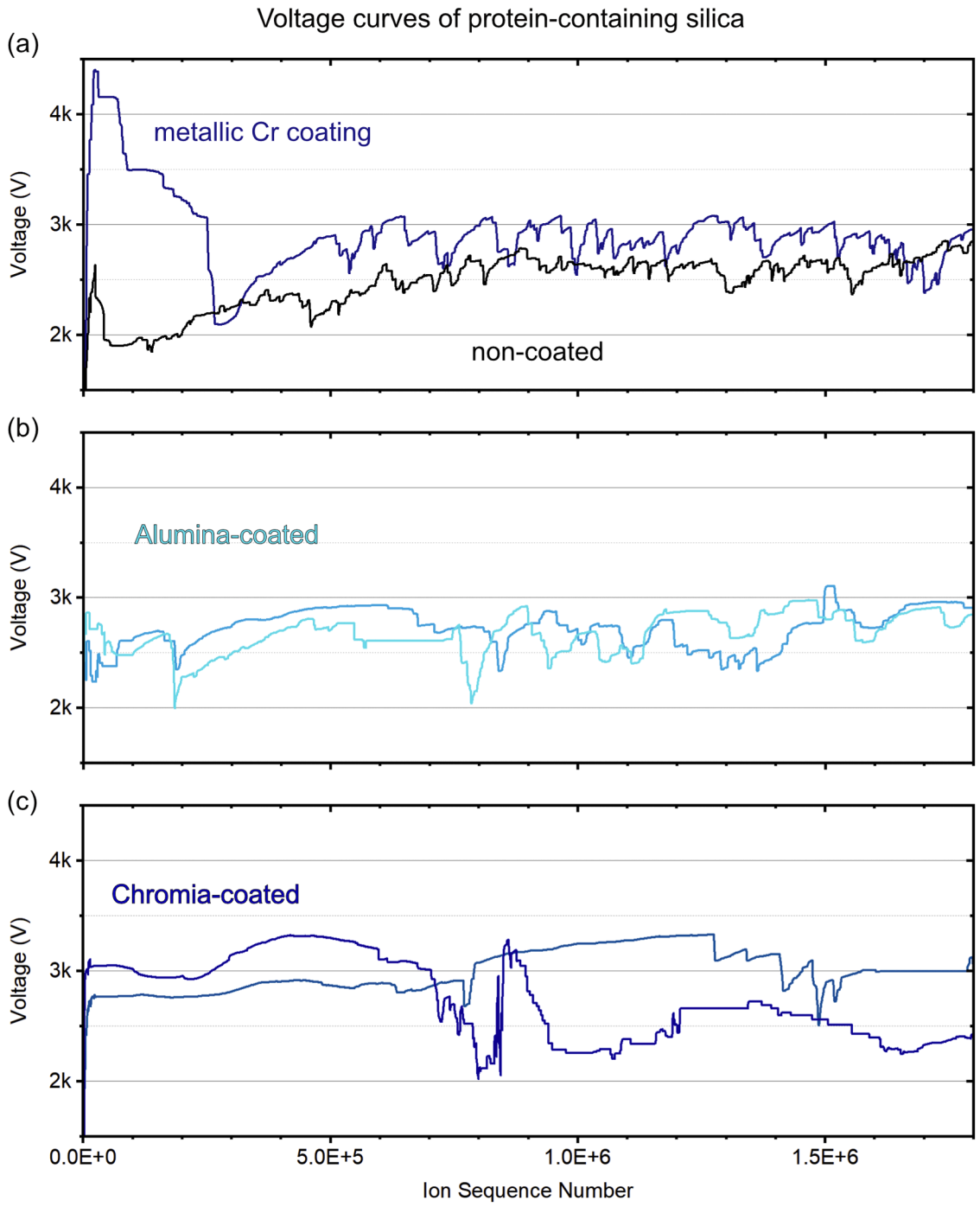

Fig. 3. APT voltage profiles of protein-containing silica specimens. (a) Uncoated specimen (black) and Cr-coated specimen. (b) Two independently measured alumina-coated specimens. (c) Two independently measured chromia-coated specimens. All measured at 50 K and 50 pJ LPE, target detection rates 0.5–2.0 %.

(see white arrows in Fig. 2b).

3.2. *Effect of oxide and metallic coatings on the evaporation behaviour*

Fig. 3 shows the voltage evolution profiles (voltage curves) obtained during APT analysis of silica specimens: (a) a comparison between a Cr coated specimen (blue) and an uncoated specimen (black), (b) two alumina-coated and (c) two chromia-coated specimens. All voltage curves exhibit regions of pronounced non-smooth behaviour, reflecting unstable ion evaporation. Because the instrument control algorithm continuously adjusts the applied voltage to maintain a target detection rate, typically 0.5–2 % (corresponding to approximately one event per 200–50 pulses), abrupt increases in evaporation rate result in a rapid reduction in the applied voltage. This produces the characteristic serrated voltage profiles observed for the silica specimens. This behaviour differs markedly from that typically observed for metals, alloys and many semiconductors or oxides that are conventionally analysed by APT, where homogenous evaporation rates produce smooth voltage curves, which enables reliable and reproducible 3D reconstructions. Recently, *in-situ* metallic coatings have been demonstrated to improve specimen yield [26] and to protect samples from environmental exposure [28], among other benefits. However, as shown in Fig. 3a, the metallic Cr coating did not significantly improve the detection rate stability for the silica specimens. Although the voltage initially increases

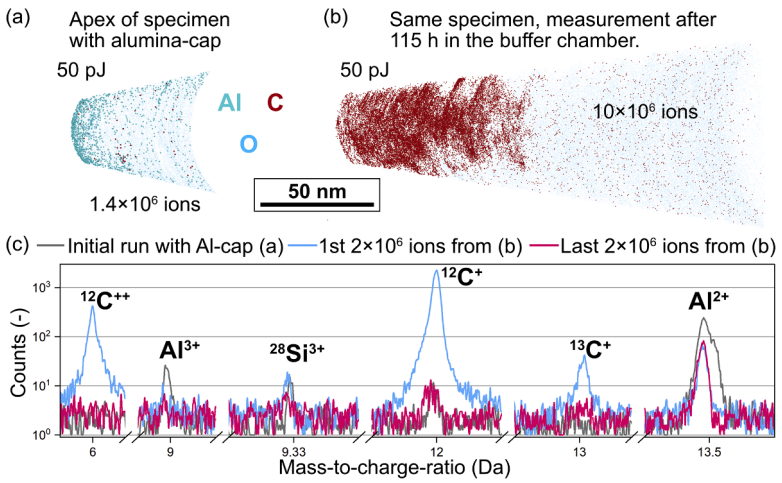

Fig. 4. ^{12}C-contamination acquired during storage in the LEAP buffer chamber: (a) Reconstruction of the first 1.4 × 10^6 detected ions from the initial experiment (see text), including the alumina coated apex region. (b) Reconstruction from a second APT experiment performed on the specimen after approximately 115 h of storage in the buffer chamber. (c) Spectra corresponding to the reconstruction in (a) and the first and last 2 × 10^6 ions detected from the reconstruction shown in (b).

relatively smoothly, a serrated pattern characteristic of the nano-porous silica emerged once the Cr coating within the field-of-view had been fully evaporated. This observation is consistent with recent studies of deep-UV laser-assisted APT, showing that oxides can evaporate at lower LPEs, or at higher rate at a given LPE, than metals [12]. This suggests that coatings with evaporation characteristics more closely matched to those of the underlying specimen may be better suited for silica, and potentially for other non-conductive or wide-bandgap materials analysed using deep-UV laser-assisted APT.

For specimens coated with alumina or chromia, sections containing several hundred thousand detected ions exhibited comparatively smooth and predominantly monotonic voltage increases, thereby satisfying an important prerequisite for reliable reconstruction. Nevertheless, the stabilizing effect of the oxide coatings was generally limited to approximately the first ~ 1 × 10^6 detected ions. At the beginning of the analysis, the coating contributes strongly to the evaporation behaviour, whereas at greater analysis depths the porous silica increasingly dominates. The resulting bursts in evaporation rate may arise from local enhancement of the electrostatic field near pores, which can promote unstable field evaporation.

3.3. Coatings prevent contamination

In addition to stabilizing the evaporation behaviour, the coatings provided a second beneficial effect by reducing the uptake of contaminant species during specimen transfer from the FIB instrument to the LEAP under ambient conditions. The ^{13}C-labelled DegP had a ^{13}C:^{12}C ratio of > 19:1 (i.e., > 95 % of all C is ^{13}C) compared with a natural abundance ratio of approximately 1:99. In contrast, the APT datasets in our previously published work [29] typically exhibited ^{13}C:^{12}C ratios ranging from approximately 1:1 to 20:1, with many datasets from ^{13}C-labelled proteins falling in the range of 5–10:1. This indicates that a substantial fraction of the detected ^{12}C originates from contamination rather than from the protein itself. Importantly, spectra of non-^{13}C-labelled IgG embedded in silica [14], acquired using the same methodology as the current DegP samples, showed carbon peaks consistent with natural abundance. Thus, only a small fraction of the 6.5 and 13 Da signals in the current experiments can be attributed to ^{12}CH species (Fig. S3). Potential sources include the synthesis and specimen-preparation procedures, for example carbon-containing precursor gases used during Pt deposition, as well as contamination acquired during transfer from the FIB to the LEAP or during storage in the load-lock and buffer chambers.

For silica specimens containing only very low levels of ^{12}C contamination after synthesis, we observed that additional carbon contamination could accumulate inside the buffer chamber of the LEAP. Fig. 4 shows reconstructions from two APT analyses performed on the same alumina-coated, protein free, specimen. Fig. 4a shows a slice through the apex region from the first analysis, when the specimen was still covered by a thin alumina layer. Fig. 4b shows a reconstruction from a subsequent analysis performed after the specimen had remained in the buffer chamber for approximately 115 h at a pressure below 3 × 10^{-9} Torr (see Fig. S 4 and S 5). The experiment was repeated twice, and in all cases significant amounts of ^{12}C were observed after storage in the buffer chamber for several days. In contrast, no comparable ^{12}C contamination was observed when specimens were kept in the analysis chamber. In the reconstruction shown in Fig. 4b, elevated ^{12}C counts were concentrated near the specimen apex, where the coating has been removed during the preceding APT analysis, whereas little or no corresponding contamination was observed further down the shank, where the coating was expected to remain intact. These observations suggest that contamination was primarily adsorbed onto the exposed silica surface at the apex, while the remaining coating provided protection against carbon uptake along the shank.

3.4. Coatings facilitate improved analysis of proteins

The ramifications of the results shown in Fig. 4 are important, as they demonstrate that it is possible to synthesize silica with very little carbon contamination (3355 contaminant C ions rather homogenously distributed in a dataset larger than 27 × 10^6 ions, i.e., ~ 0.01 ionic %). Furthermore, the results also show that specimens that are not *in situ* coated (or where the coating is removed as demonstrated above) accumulate substantial amounts of ^{12}C during storage inside the buffer chamber. Because this contamination occurred even at pressures of approximately 10^{-9} Torr, it is reasonable to expect that uncoated specimens may also acquire carbon contamination during transfer from the FIB to the LEAP under ambient conditions (and during storage in the buffer chamber). We attribute this to the large specific surface area (generally in the range of 500 m^2/g) of the interconnected network of pores inside the silica, which facilitates the ingress from adsorbed contaminants at the shank into the 'bulk' of the needle specimens. Consequently, a substantial fraction of the ^{12}C detected in uncoated specimens is likely to originate from contamination rather than from the embedded proteins. Importantly, the workflow established here provides a *non-cryogenic* route for substantially reducing carbon contamination. This is particularly relevant for future APT analysis of non-isotopically labelled organic material, for which reliable discrimination between

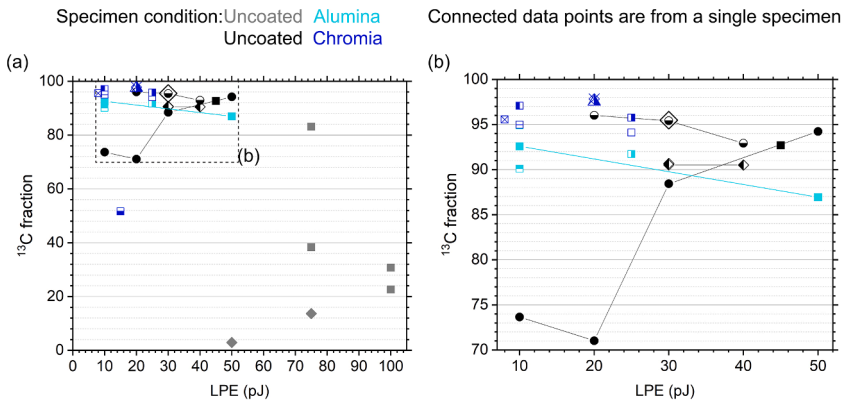

Fig. 5. Measured percentage of ^{13}C (^{13}C /(^{12}C + ^{13}C)) in uncoated, chromia- and alumina-coated DegP-containing silica specimens. Each symbol represents an individual APT specimen. (a) depicts all data and (b) is an enlarged view of the dashed region in (a) for improved visibility.

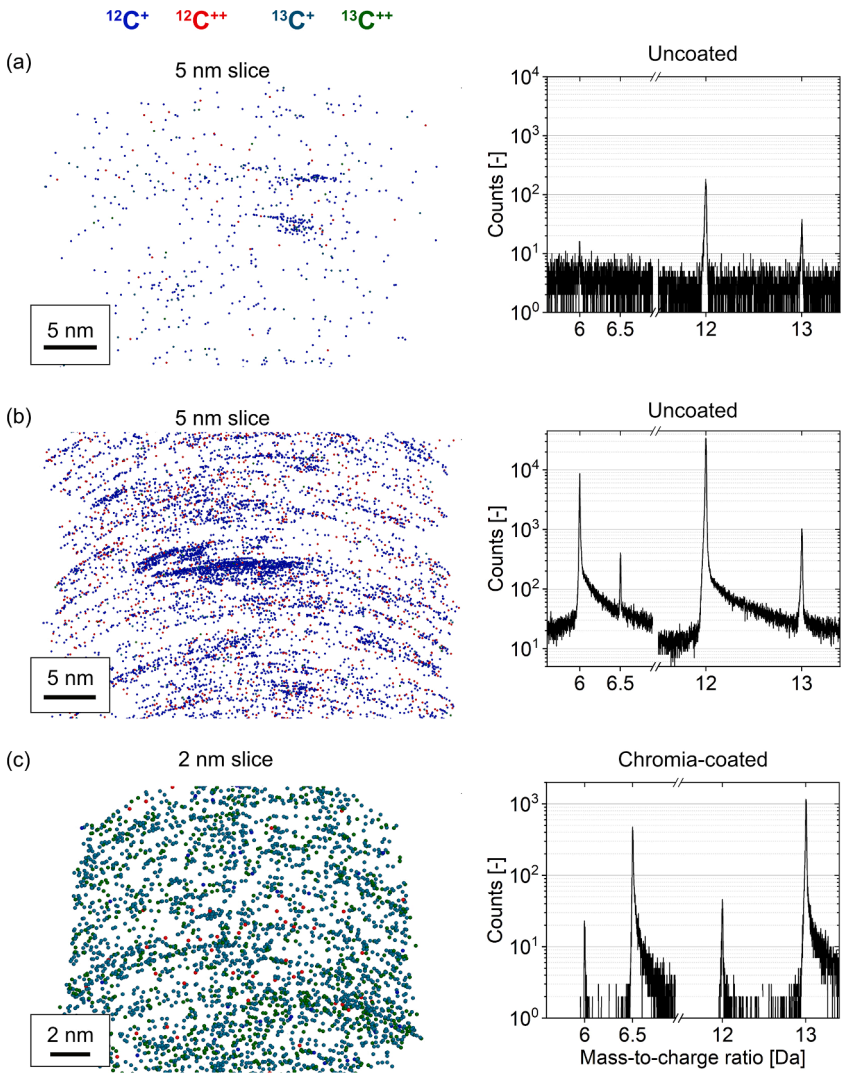

Fig. 6. Comparison of APT reconstructions and corresponding mass-to-charge spectra from (a, b) uncoated and (c) chromia-coated DegP specimens. All measurements were performed at 50 K and an LPE of 50 pJ.

specimen-derived carbon and adventitious carbon is essential.

Fig. 5 presents data from six lift-outs (three uncoated, one with alumina and two with chromia coated specimens), each yielding 4–6 APT specimens (see details in Table S1). It comprises plots of the measured ^{13}C fraction of the carbon detected at 6, 6.5, 12, and 13 Da, i.e., all non-molecular carbon ions, as a function of LPE. Data points connected by lines correspond to measurements from the same needle specimen acquired at different LPEs. The plots show a striking difference between the ^{13}C-fractions measured in uncoated specimens (grey and black symbols) and those coated with alumina (light blue) or chromia

(dark blue) specimens. The data from almost all coated specimens show ^{13}C-fractions of 90 % or higher, with the chromia-coated specimens generally exceeding 95 % (except for one outlier, a single specimen – see the half-filled blue square around 50 % – where no Cr could be detected in the spectrum, i.e., the coating process was not effective). In contrast, the uncoated specimens exhibit ^{13}C fractions from approximately 2 % to 96 %. In addition to the pronounced variability of the detected ^{13}C-fraction between lift-outs (see the difference between black and grey data points), there is significantly higher spread for non-coated specimens as is seen in the cases represented by the filled black circles.

Fig. 6 further illustrates the results obtained from uncoated (a and b) and chromia-coated (c) specimens by showing slices through the APT reconstructions together with the corresponding regions of the mass-to-charge spectra where the elemental C peaks are located. Fig. 6(a) and (b) illustrate the considerable variation in carbon content between individual uncoated specimens. In both cases, ^{12}C is more abundant than ^{13}C. The observed clustering of carbon further emphasizes the importance of minimizing contaminant carbon ingress as such clusters could otherwise be falsely identified as originating from proteins by commonly used clustering algorithms. In addition, the reconstruction in Fig. 6b exhibits a characteristic distribution of carbon ions indicative of preferential evaporation. This is evident from the ions aligned like *pearls-on-a-string*-like features that approximately follow the curvature of the specimen surface. A similar effect is observed in the ^{13}C containing volume depicted in Fig. 6c albeit to a lesser extent. The ^{13}C distribution also demonstrates that individual proteins cannot be resolved under the present conditions. To enable identification of individual proteins and extraction of structural and chemical information at the single-protein level, the proteins must be distributed sufficiently homogeneously within the silica matrix and spatially separated from one another. Achieving such a distribution has, however, proven challenging during sample preparation, as has also been reported for cryo-electron microscopy samples [30]. Further optimization of the embedding procedure and strategies to suppress protein aggregation will therefore be required.

4. Conclusions

We demonstrate that protein-containing specimens can be prepared by encapsulation in porous silica and successfully analysed by APT, while in situ oxide coatings of alumina or chromia effectively suppress carbon contamination. This substantially reduces interference from adventitious carbon and expands the potential of the approach beyond the analysis of isotopically labelled proteins. The oxide coatings also promoted more stable and homogeneous field evaporation, as reflected by smoother voltage curves, representing an important improvement over previous studies and a prerequisite for more reliable spatial reconstruction.

Despite these advances, the aggregation of proteins during sample preparation prevented the identification and structural characterization of individual protein molecules in the present datasets. Achieving a sufficiently homogeneous and well-separated distribution of proteins within the silica matrix will therefore be essential for progressing towards three-dimensional structural analysis of individual proteins by APT. In addition, the intrinsic porosity of the silica matrix remains a challenge for accurate 3D reconstruction. Future work should therefore focus on improving control over protein distribution and reducing or eliminating matrix porosity, for example through suitable pore-backfilling strategies.

CRediT authorship contribution statement

David Mayweg: Writing – original draft, Methodology, Formal analysis, Conceptualization. **Gustav Eriksson:** Writing – review & editing, Formal analysis, Data curation. **Annija Stepulane:** Writing – review & editing, Methodology, Data curation. **Darius Šulskis:** Writing – review & editing, Formal analysis, Data curation. **Björn M. Burmann:** Writing – review & editing, Methodology, Conceptualization. **Per Malmberg:** Writing – review & editing, Formal analysis, Data curation. **Mattias Thuvander:** Writing – review & editing, Formal analysis. **Mats Hulander:** Writing – review & editing, Methodology, Formal analysis. **Martin Andersson:** Writing – review & editing, Supervision, Funding acquisition, Conceptualization.

Declaration of competing interest

The authors declare that they have no known competing financial interests or personal relationships that could have appeared to influence the work reported in this paper.

Acknowledgements

This research has received funding from the European Union under the Mimosa grant agreement No 101046651. This work has also been funded by the Swedish Innovation Agency Vinnova under the acceleration of deep tech companies program (2024–02265). The experimental work was carried out at Chalmers Materials Analysis Laboratory (CMAL) at Chalmers University of Technology in Gothenburg. The ToF-SIMS investigations were carried out using the Chemical Imaging Infrastructure (CII) Research and Technology Platform, which was funded by the Knut and Alice Wallenberg Foundation via the Wallenberg Initiative Materials Science for Sustainability (WISE).

Supplementary materials

Supplementary material associated with this article can be found, in the online version, at doi:10.1016/j.sampre.2026.100262.

Data availability

Data will be made available on request.

References

[1] A. McPherson, J.A. Gavira, Introduction to protein crystallization, Acta Crystallogr. F. Struct. Biol. Commun. 70 (Pt 1) (2014) 2–20.
[2] M.A. Herzik Jr., M. Wu, G.C. Lander, High-resolution structure determination of sub-100 kDa complexes using conventional cryo-EM, Nat. Commun. 10 (1) (2019) 1032.
[3] R.M. Glaeser, How good can single-particle cryo-EM become? What remains before it approaches its physical limits? Annu Rev. Biophys. 48 (2019) 45–61.
[4] K. Takeuchi, K. Baskaran, H. Arthanari, Structure determination using solution NMR: is it worth the effort? J. Magn. Reson. 306 (2019) 195–201.
[5] A.R. Camacho-Zarco, V. Schnapka, S. Guseva, A. Abyzov, W. Adamski, S. Milles, M. R. Jensen, L. Zidek, N. Salvi, M. Blackledge, NMR provides unique insight into the functional dynamics and interactions of intrinsically disordered proteins, Chem. Rev. 122 (10) (2022) 9331–9356.
[6] B.M. Burmann, S. Hiller, Chaperones and chaperone-substrate complexes: dynamic playgrounds for NMR spectroscopists, Prog. Nucl. Magn. Reson. Spectrosc. 86-87 (2015) 41–64.
[7] S. Muniyappan, Y. Lin, Y.H. Lee, J.H. Kim, ^{17}O NMR spectroscopy: a novel probe for characterizing protein structure and folding, Biol. (Basel) 10 (6) (2021).
[8] B. Gault, A. Chiaramonti, O. Cojocaru-Mirédin, P. Stender, R. Dubosq, C. Freysoldt, S.K. Makineni, T. Li, M. Moody, J.M. Cairney, Atom probe tomography, Nat. Rev. Methods Primers 1 (1) (2021) 51.
[9] T.F. Kelly, O. Nishikawa, J.A. Panitz, T.J. Prosa, Prospects for nanobiology with atom-probe tomography, MRS Bull. 34 (10) (2009) 744–750.
[10] T.T. Tsong, Pulsed-laser-stimulated field ion emission from metal and semiconductor surfaces: a time-of-flight study of the formation of atomic, molecular, and cluster ions, Phys. Rev. B 30 (9) (1984) 4946–4961.
[11] B.W. Caplins, A.N. Chiaramonti, J.M. Garcia, N.A. Sanford, L. Miaja-Avila, Atom probe tomography using an extreme ultraviolet trigger pulse, Rev. Sci. Instrum. 94 (9) (2023).
[12] S. Jakob, J.D. Poplawsky, A.S. Jelinek, D. Mayweg, M. Thuvander, Potential role of hole accumulation via photoionization and electron tunneling during laser-assisted field evaporation of insulators with high energy photons, Phys. Rev. B 112 (16) (2025).
[13] M.A. Cianfrocco, E.H. Kellogg, What could go wrong? A practical guide to single-particle cryo-EM: from biochemistry to atomic models, J. Chem. Inf. Model. 60 (5) (2020) 2458–2469.

[14] G. Sundell, M. Hulander, A. Pihl, M. Andersson, Atom probe tomography for 3D structural and chemical analysis of individual proteins, Small 15 (24) (2019) e1900316.
[15] D.E. Perea, J. Liu, J. Bartrand, Q. Dicken, S.T. Thevuthasan, N.D. Browning, J. E. Evans, Atom probe tomographic mapping directly reveals the atomic distribution of phosphorus in resin embedded ferritin, Sci. Rep. 6 (2016) 22321.
[16] K.A.K. Rusitzka, L.T. Stephenson, A. Szczepaniak, L. Gremer, D. Raabe, D. Willbold, B. Gault, A near atomic-scale view at the composition of amyloid-beta fibrils by atom probe tomography, Sci. Rep. 8 (1) (2018) 17615.
[17] S. Zhang, L.S. Aota, M.P. Singh, E.V. Woods, F. Perier Jouet, T.M. Schwarz, B. Gault, Atom probe tomography of hydrated biomacromolecules: preliminary results, Microscopy and microanalysis : the official journal of Microscopy Society of America, Microbeam Analysis Society, Microsc. Soc. Can. 31 (4) (2025).
[18] E.V. Woods, T.M. Schwarz, M.P. Singh, S. Zhang, S.H. Kim, A.A. El-Zoka, L. Gremer, D. Willbold, I. McCarroll, B. Gault, Mapping the path to cryogenic atom probe tomography Analysis of biomolecules, Microscopy and microanalysis : the official journal of Microscopy Society of America, Microbeam Analysis Society, Microsc. Soc. Can. 31 (4) (2025).
[19] L.T. Stephenson, A. Szczepaniak, I. Mouton, K.A.K. Rusitzka, A.J. Breen, U. Tezins, A. Sturm, D. Vogel, Y. Chang, P. Kontis, A. Rosenthal, J.D. Shepard, U. Maier, T. F. Kelly, D. Raabe, B. Gault, The Laplace Project: an integrated suite for preparing and transferring atom probe samples under cryogenic and UHV conditions, PLoS. One 13 (12) (2018) e0209211.
[20] D. Šulskis, J. Thoma, B.M. Burmann, Structural basis of DegP protease temperature-dependent activation, Sci. Adv. 7 (50) (2021) eabj1816.
[21] T. Clausen, M. Kaiser, R. Huber, M. Ehrmann, HTRA proteases: regulated proteolysis in protein quality control, Nat. Rev. Mol. Cell Biol. 12 (3) (2011) 152–162.
[22] R.B. Bhatia, C.J. Brinker, A.K. Gupta, A.K. Singh, Aqueous sol−gel process for protein encapsulation, Chem. Mater. 12 (8) (2000) 2434–2441.
[23] D.M. Liu, I.W. Chen, Encapsulation of protein molecules in transparent porous silica matrices via an aqueous colloidal sol–gel process, Acta Mater. 47 (18) (1999) 4535–4544.
[24] B. Gault, D. Haley, F. de Geuser, M.P. Moody, E.A. Marquis, D.J. Larson, B. P. Geiser, Advances in the reconstruction of atom probe tomography data, Ultramicroscopy 111 (6) (2011) 448–457.
[25] K. Thompson, D. Lawrence, D.J. Larson, J.D. Olson, T.F. Kelly, B. Gorman, In situ site-specific specimen preparation for atom probe tomography, Ultramicroscopy 107 (2–3) (2007) 131–139.
[26] T.M. Schwarz, E. Woods, M.P. Singh, X. Chen, C. Jung, L.S. Aota, K. Jang, M. Kramer, S.H. Kim, I. McCarroll, B. Gault, In-situ metallic coating of atom probe specimen for enhanced yield, performance, and increased field-of-view. Microscopy and Microanalysis : the Official Journal of Microscopy Society of America, Microbeam Analysis Society, Microscopical Society of Canada, 2024.
[27] B. Gault, A. Saksena, X. Sauvage, P. Bagot, L.S. Aota, J. Arlt, L.T. Belkacemi, T. Boll, Y.S. Chen, L. Daly, M.B. Djukic, J.O. Douglas, M.J. Duarte, P.J. Felfer, R.G. Forbes, J. Fu, H.M. Gardner, R. Gemma, S.S.A. Gerstl, Y. Gong, G. Hachet, S. Jakob, B. M. Jenkins, M.E. Jones, H. Khanchandani, P. Kontis, M. Kramer, M. Kuhbach, R.K. W. Marceau, D. Mayweg, K.L. Moore, V. Nallathambi, B.C. Ott, J.D. Poplawsky, T. Prosa, A. Pundt, M. Saha, T.M. Schwarz, Y. Shang, X. Shen, M. Vrellou, Y. Yu, Y. Zhao, H. Zhao, B. Zou, Towards establishing best practice in the analysis of hydrogen and deuterium by atom probe tomography. Microscopy and Microanalysis : the Official Journal of Microscopy Society of America, Microbeam Analysis Society, Microscopical Society of Canada, 2024.
[28] M.P. Singh, E.V. Woods, S.-H. Kim, C. Jung, L.S. Aota, B. Gault, Facilitating the systematic nanoscale study of battery materials by atom probe tomography through in-situ metal coating, Batter. Supercaps 7 (2) (2024) e202300403.
[29] G. Eriksson, D. Mayweg, G.N. Inverardi, F. Carnovale, M. Hulander, M. Thuvander, L. Petrolli, G. Lattanzi, S. Taioli, M. Andersson, Silica-embedded proteins enable higher yield and atomic ion detection in deep-UV laser-assisted atom probe tomography, Anal. Chem. 98 (33) (2026) 24290–24302.
[30] I. Drulyte, R.M. Johnson, E.L. Hesketh, D.L. Hurdiss, C.A. Scarff, S.A. Porav, N. A. Ranson, S.P. Muench, R.F. Thompson, Approaches to altering particle distributions in cryo-electron microscopy sample preparation, Acta Crystallogr. D. Struct. Biol. 74 (Pt 6) (2018) 560–571.